JOURNAL OF VIROLOGY, Dec. 2003, p. 13275–13287 Vol. 77, No. 24
0022-538X/03/$08.00+0 DOI: 10.1128/JVI.77.24.13275–13287.2003

Association of Adenovirus with the Microtubule Organizing Center

Christopher J. Bailey,[1,2] Ronald G. Crystal,[1] and Philip L. Leopold[1]*

Department of Genetic Medicine[1] and Program in Neuroscience, Weill Graduate School of Medical Sciences,[2] Weill Medical College of Cornell University, New York, New York

Received 12 March 2003/Accepted 15 September 2003

Adenoviruses (Ad) must deliver their genomes to the nucleus of the target cell to initiate an infection. Following entry into the cell and escape from the endosome, Ad traffics along the microtubule cytoskeleton toward the nucleus. In the final step in Ad trafficking, Ad must leave the microtubule and establish an association with the nuclear envelope. We hypothesized that in cells lacking a nucleus, the capsid moves to and associates with the microtubule organizing center (MTOC). To test this hypothesis, we established an experimental system to examine Ad trafficking in enucleated cells compared to Ad trafficking in intact, mock-enucleated cells. Enucleation of a monolayer of A549 human lung epithelial cells was accomplished by depolymerization of the actin cytoskeleton followed by centrifugation. Upon infection of enucleated cells with Cy3-labeled Ad, the majority of Ad capsid trafficked to a discrete, centrally located site which colocalized with pericentrin, a component of the MTOC. MTOC-associated Ad had escaped from endosomes and thus had direct access to MTOC components. Ad localization at this site was sensitive to the microtubule-depolymerizing agent nocodazole, but not to the microfilament-depolymerizing agent cytochalasin B, indicating that intact microtubules were required to maintain the localization with the MTOC. Ad localization to the MTOC in the enucleated cells was stable, as demonstrated by continuing Ad localization with pericentrin for more than 5 h after infection, a strong preference for Ad arrival at rather than Ad departure from the MTOC, and minimal redistribution of Ad between MTOCs within a single cell. In summary, the data demonstrate that the Ad capsid establishes a stable interaction with the MTOC when a nucleus is not present, suggesting that dissociation of Ad from microtubules likely requires nuclear factors.

The remarkable efficiency with which adenovirus serotype 5 (Ad) targets its genetic cargo to the nuclei of cells results from a coordinated series of interactions between the Ad capsid and cellular organelles (6, 39). Implicit in this pathway is the need for Ad to extricate itself from each preceding interaction so that each subsequent interaction may occur. The initial step of Ad infection is characterized by the association of capsid proteins with cell surface receptors, specifically a primary high-affinity interaction between the Ad fiber protein and the coxsackie-adenovirus receptor (CAR) followed by a secondary interaction between RGD sequences in the penton base protein and cell surface integrins (2, 4, 11, 19, 46, 49, 50). After entry of Ad into the cell via receptor-mediated endocytosis, Ad lyses the surrounding endosomal membrane and detaches from its receptors through programmed release of penton capsomeres, including the fiber and penton base proteins (13, 15, 21, 30, 32, 44, 48). The virus then undergoes cytoplasmic dynein-dependent trafficking along microtubules toward the nucleus (22, 24, 43). Ultimately, the capsid forms a stable association with the nuclear envelope, where the Ad genome disengages from the capsid, leaving an empty capsid (7, 10). After leaving the capsid, the Ad genome with its associated DNA binding proteins moves through a nuclear pore and enters the nucleus, where it utilizes endogenous nuclear enzymes to transcribe the Ad genome (16, 38, 47, 51).

Among these processes, the transition from microtubule translocation to nuclear binding requires further characterization. The microtubule cytoskeleton forms a coordinate system within the cell originating at the microtubule organizing center (MTOC) and radiating toward the cell periphery. The microtubule cytoskeleton controls the positioning of many organelles within the cell, including the Golgi apparatus, lysosomes, endosomes, and the nucleus, which is often found in close apposition to the MTOC (45). The MTOC contains a unique complement of proteins, including pericentrin, α-, β-, and γ-tubulin, Spc97p, 98c, 110p, γ-tubulin binding protein, centrin, ninein, CDC2, CPAP, kendrin, protein kinase A, dynactin, and cytoplasmic dynein (5). Microtubules have an inherent polarity, with the slow-growing (negative) end toward the MTOC and the fast-growing (positive) end toward the cell periphery (26, 27, 37). The microtubule-dependent molecular motor, cytoplasmic dynein, moves cargo toward the MTOC and the nucleus (40). Intracellular trafficking of Ad is known to involve cytoplasmic dynein movement toward the MTOC (22, 43), but at some point during this process, Ad suspends its microtubule-dependent translocation in favor of a stable association with the nuclear envelope.

There are hints that the Ad capsid may associate with the MTOC prior to translocation to the nucleus. Ad accumulates in juxtaposition with the nucleus near the MTOC prior to binding to the nuclear envelope in some cell types (14). However, the proximity of the MTOC to the nuclear envelope complicates the analysis of Ad-MTOC interaction compared to Ad-nuclear envelope interaction. When Ad infects mitotic cells that lack intact nuclei, the Ad capsid accumulates at MTOC structures (spindle poles) (10, 22). However, since dissociated elements of the nuclear envelope also accumulate at spindle

* Corresponding author. Mailing address: Department of Genetic Medicine, Weill Medical College of Cornell University, 515 East 71st St., S-1000, New York, NY 10021. Phone: (212) 746-2258. Fax: (212) 746-8383. E-mail: geneticmedicine@med.cornell.edu.

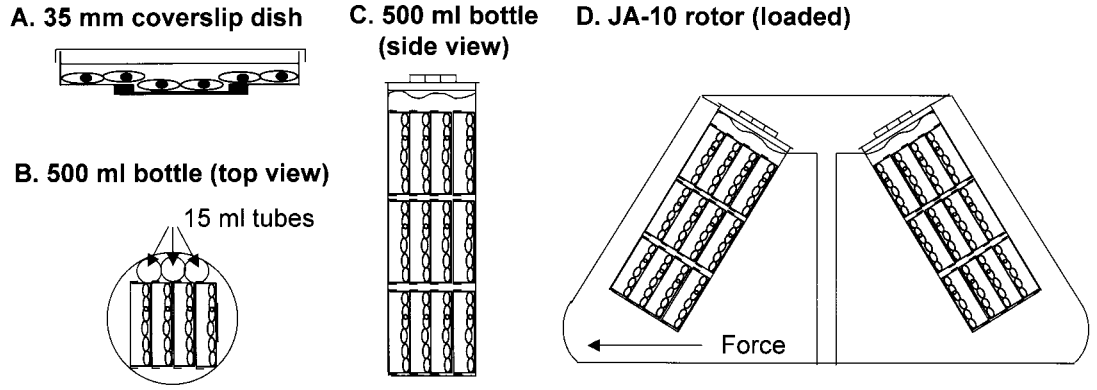

FIG. 1. Method for producing enucleated cells. A549 cells were plated and grown on coverslip dishes (see reference 21). Cells to be enucleated were treated with cytochalasin B medium and mock-enucleated cells were treated with control medium and centrifuged identically. (A) A549 cells in 35-mm-diameter coverslip dish. Cells at the center of the dish grow on an optical quality coverslip that is adhered to the bottom of the 35-mm-diameter dish to cover a hand-punched hole. (B) Top view of 500-ml centrifuge bottle loaded with stacks of dishes, each containing four coverslip dishes and three 15-ml centrifuge tubes to lock the coverslip dishes into place. (C) Side view of 500-ml centrifuge bottle loaded with three stacks of coverslip dishes. All of the dishes are submerged in medium. (D) Centrifuge rotor diagram with 500-ml centrifuge bottles containing coverslip dishes for enucleation. Note that the monolayers are oriented so that the direction of centrifugal force is nearly perpendicular to the monolayer.

poles, it is unclear whether Ad interacts with the constituents of the MTOC or with the dissociated elements of the nuclear envelope. To evaluate the hypothesis that Ad capsids form a stable association with the MTOC during the trafficking process, we developed a model system for Ad trafficking in enucleated cells. The data demonstrate that there is a stable association of Ad with the MTOC in the absence of a nucleus. The results have implications for understanding the mechanism of transition from microtubule-based translocation to a stable nuclear envelope association during viral infection.

MATERIALS AND METHODS

Cell culture and enucleation. A549 human lung epithelial carcinoma cells (American Type Culture Collection, Rockville, Md.) were cultured in Dulbecco's modified Eagle's medium (DMEM; Invitrogen, Carlsbad, Calif.) supplemented with 10% fetal bovine serum (Invitrogen), penicillin (100 U/ml; Life Technologies, Gaithersburg, Md.), streptomycin (100 U/ml; Life Technologies), and 1% fungizone (Biofluids, Rockville, Md.). For microscopy experiments, cells were cultured on poly-D-lysine-coated coverslips affixed to 35-mm-diameter tissue culture dishes as described previously (21). The cells were seeded at 10^6 cells per 35-mm-diameter dish, incubated at 37°C in a humidified incubator with 5% CO_2, and used 24 h after plating. Enucleation of cell monolayers was performed by a method modified from earlier reports (9, 33). Cells cultured on coverslip dishes were enucleated by the addition of DMEM containing 20 μM (10 μg/ml) cytochalasin B (Sigma, St. Louis, Mo.) and by centrifugation in 500-ml centrifuge bottles (Nalgene, Rochester, N.Y.) at 37°C for 60 min at 7,250 × *g* in a Beckman centrifuge with a JA-10 rotor (Beckman, Palo Alto, Calif.). The coverslip dishes were assembled into three stacks containing four coverslip dishes each. The stacks were loaded into the 500-ml centrifuge bottles such that the plane of the monolayers was nearly perpendicular to the direction of centrifugal force. Three 15-ml conical centrifuge tubes were used to fill excess space in the 500-ml bottle (Fig. 1). Mock-enucleated cells were treated with DMEM without cytochalasin B and centrifuged as described above. To ensure viability of the cellular system during experiments, cellular respiration was characterized by use of MitoTracker Red dye (Molecular Probes, Inc., Eugene, Oreg.), a dye which is accumulated and retained in the mitochondria of respiring cells. Naive, mock-enucleated, and enucleated cells were incubated for 0 to 9 h postcentrifugation and -enucleation in fresh medium, loaded with MitoTracker Red dye (100 nM for 15 min at 37°C) in DMEM, and then washed three times with fresh medium and three times with phosphate-buffered saline (PBS) and fixed at −20°C for 20 min with methanol (Sigma). To confirm the validity of the MitoTracker Red staining, naive, mock-enucleated, and enucleated cells were treated with medium containing 0.1% sodium azide (Sigma) for 30 min at 37°C followed by the MitoTracker Red staining procedure. The enucleation protocol was optimized, resulting in the protocol described above. During the optimization procedure, the actin depolymerization agent cytochalasin D (Sigma) was used at the same concentration as cytochalasin B (8). Latrunculin A (Calbiochem, La Jolla, Calif.) and latrunculin B (Calbiochem) were also tested for the enucleation protocol at concentrations previously reported to induce actin depolymerization (10 and 100 nM) (42). Additionally, we tested nocodazole (5 and 25 μM) (Sigma) as an agent for creating enucleated cells by depolymerizing the microtubule cytoskeleton (23). For obtaining the optimum enucleation protocol, centrifugation speeds (6,000, 6,500, 6,750, 7,000, 7,250, 7,500, and 8,000 × *g*), times (50, 55, 60, 65, 70, and 90 min), temperatures (4, 14, 24, 34, and 37°C), and angles of orientation (90 and 180° from the angle of force) were investigated.

Adenovirus vector. AdNull is an $E1^-$, $E3^-$, replication-deficient serotype 5 vector that contains the cytomegalovirus early-intermediate enhancer-promoter with no transgene (17). The vector was prepared and stored at −80°C as described previously (35, 36). The concentration of virus particles was determined by measuring the absorbance at 260 nm and using the extinction coefficient for Ad (9.09×10^{-13} ml/cm of particle) (28). The fluorophores Cy3 (Amersham Life Sciences Inc., Arlington Heights, Ill.) and carboxyfluorescein (Molecular Probes) were covalently conjugated to the Ad capsid by succinimidyl ester chemistry as described previously (29). Fluorophore-conjugated vectors were stored at −20°C in a 30% glycerol stock (Sigma).

Infection of mock-enucleated or enucleated A549 cells with fluorophore-conjugated Ad. Cells were washed three times in binding buffer (1× minimum essential medium [MEM; Invitrogen], 1% bovine serum albumin [BSA; Sigma], 10 mM HEPES [Biofluids] [pH 7.4]). Naive, mock-enucleated, or enucleated cells were infected with Cy3-Ad or carboxyfluorescein-Ad (10^{11} particles/ml, 10 min, 37°C) in binding buffer. After infection, unbound Ad was removed by three washes with binding buffer followed by a 60-min incubation at 37°C. Following incubation, cells were washed three times with PBS (Biofluids) and fixed in −20°C methanol (Sigma) for 20 min. After three PBS washes, the nuclei were stained with 4′,6-diamidino-2-phenylindole dihydrochloride (DAPI; Molecular Probes).

Evaluation of enucleated cell structure by indirect immunofluorescence. To evaluate enucleated cell structure, we looked at the cytoskeletal elements by indirect immunofluorescence. Following fixation with methanol as described above, cells were washed three times in PBS and blocked with a solution containing 5% goat serum (Jackson Immuno Labs, Garden Grove, Pa.) and 1% BSA in PBS with 0.05% saponin (Sigma) for 20 min at 23°C. For structural analysis, primary antibodies included a rat anti-tubulin monoclonal antibody (clone YL1/2; kindly provided by Gregg Gundersen, Columbia University College of Physicians and Surgeons, New York, N.Y.), an anti-cytokeratin mouse monoclonal antibody (10 μg of purified immunoglobulin G per ml) (clone Cy-90; Sigma), and an anti-vimentin mouse monoclonal antibody (10 μg of purified immuno-

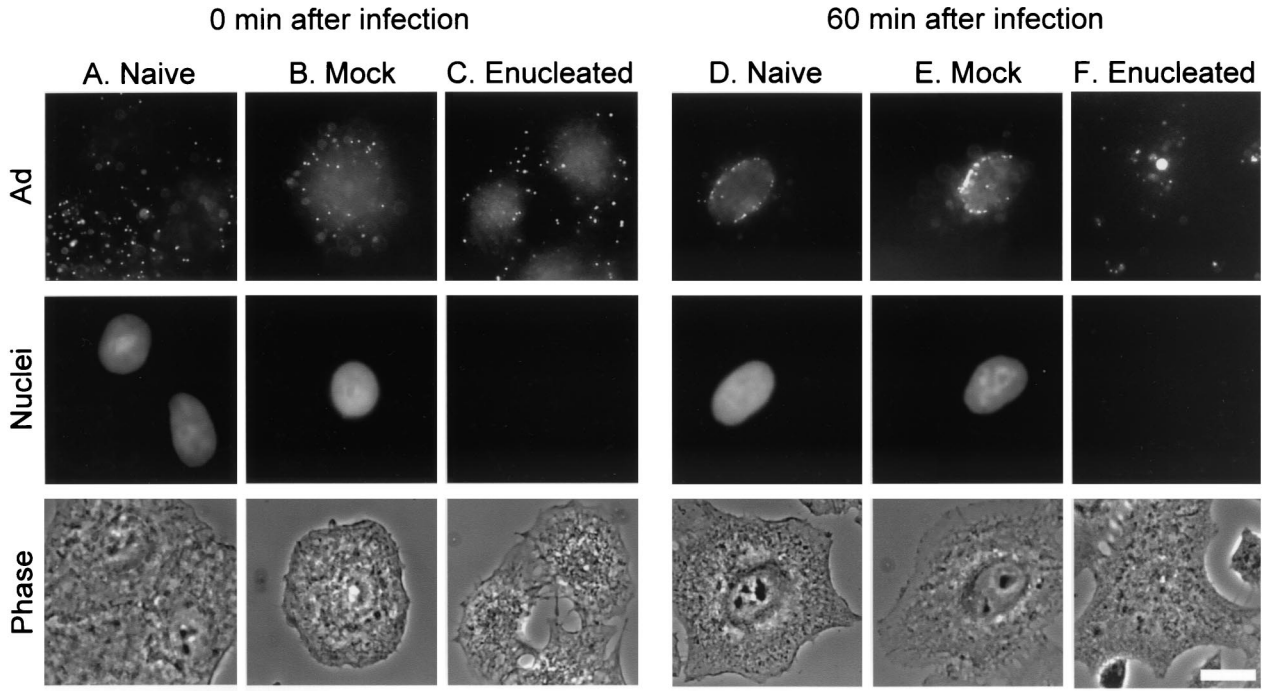

FIG. 2. Ad trafficking patterns in the presence or absence of a nucleus. Enucleated cells were prepared by treatment with cytochalasin B medium and centrifugation followed by washing. Mock-enucleated cells were centrifuged in medium lacking cytochalasin B. Following centrifugation, cells were infected with Cy3-Ad, washed, and incubated for 0 or 60 min at 37°C. Cells were fixed and the nuclei were stained with DAPI. Cy3-Ad distribution was evaluated by fluorescence and phase-contrast microscopy. (A) Naive cells 0 min after infection. (B) Mock-enucleated cells 0 min after infection. (C) Enucleated cells 0 min after infection. (D) Naive cells 60 min after infection. (E) Mock-enucleated cells 60 min after infection. (F) Enucleated cells 60 min after infection. Each panel shows Cy3-Ad (Ad), DAPI-staining (nuclei), and phase-contrast (phase) images. Bar = 10 μm.

globulin G per ml) (Chemicon, Temecula, Calif.). Each primary antibody was incubated with enucleated cells in blocking solution for 45 min at 23°C. The cells were then washed three times with 1% BSA in PBS. A goat anti-rabbit secondary antibody conjugated to Alexa 488 fluorophore was used at a final concentration of 10 μg/ml diluted in blocking solution and was incubated for 30 min at 23°C (Molecular Probes). After three washes with PBS, the nuclei were stained with DAPI as described above and were given a final three washes in PBS prior to mounting with a glycerol-based mounting medium (SlowFade; Molecular Probes). Filamentous actin structure was evaluated in enucleated cells by use of phalloidin conjugated to Alexa 488 or Alexa 546 fluorophore (220 nM, 20 min) (Molecular Probes). Phalloidin-stained cells were fixed in either 4% paraformaldehyde (Electron Microscopy Sciences, Fort Washington, Pa.) in PBS, as suggested by Molecular Probes, or methanol to allow simultaneous pericentrin staining with equivalent results.

Microscopy. Fluorescence microscopy was performed with an Olympus XL70 inverted microscope equipped with ×60 numeric aperture (N.A.) 1.40 PlanApo and ×100 N.A. 1.35 UPlanApo objective lenses. Images were acquired with a Photometrix Quantix 57 cooled charge-coupled device camera with a 535 by 512, back-illuminated, UV-VIS coated chip operating at 3 MHz (Roper Instruments, Inc., Trenton, N.J.). Image analysis was performed with Metamorph imaging software (Universal Imaging, Downingtown, Pa.). During live cell microscopy, cells were incubated in coverslip dishes with 2 ml of Leibovitz's medium (Invitrogen) supplemented with 1% BSA and 10 mM HEPES, pH 7.4, and maintained at 37°C by a Nikon NP-2 thermostat-controlled stage heater (Morrell Instruments, Melville, N.Y.). Infected cells were imaged at 40 to 60 min postinfection to determine the velocity of Ad as it undergoes intracellular trafficking prior to reaching the terminal target. Time-lapse series were acquired at 0.4-s intervals for 90 s. Image sequences were converted to a single digital video file to allow movie playback and identification of Ad particles undergoing trafficking. Ad particles that translocated in a curvilinear manner in the plane of focus for a minimum of 2 s or 2 μm of uninterrupted movement were used for velocity measurements. To evaluate stable versus labile association of Ad with the nuclear envelope or MTOC, the frequency of Ad particle arrival and departure was determined by use of time-lapse microscopy of Ad in mock-enucleated or enucleated cells. Cells were imaged at either 40 to 60 min postinfection or 60 to 90 min postinfection. Viral particles that translocated in a curvilinear manner, either arriving at or departing from the nucleus or MTOC, were scored as having movement when unidirectional translocation was observed for at least 2 s or 2 μm. Data are presented as numbers of events per minute of observation. For each condition, 15 min of time-lapse images were recorded and analyzed during the 40- to 60-min period and 15 min of time-lapse images were recorded and analyzed during the 60- to 90-min period. Each condition was analyzed for at least 10 individual cultures. Mean values for arrival and departure frequencies for each culture were determined, and the average of the means with standard error is reported for each condition.

Ad trafficking patterns in the presence or absence of a nucleus. Naive, mock-enucleated, and enucleated cells were prepared and infected as described above. The cells were then incubated for 0 or 60 min at 37°C. Following incubation, the cells were fixed and the nuclei were stained as described above. The positions of the labeled Ad were evaluated and compared to the positions of the nuclei.

Ad trafficking to the MTOC in the absence of a nucleus. Mock-enucleated and enucleated cells were prepared and infected as described above. The cells were then incubated for 60 min at 37°C. Following incubation, the cells were fixed and the MTOC was localized and detected by using indirect immunofluorescence staining as described above. To localize pericentrin, fixed cells were treated with a rabbit anti-pericentrin polyclonal antiserum (Covance, Princeton, N.J.) at a 1:150 dilution in blocking solution for 45 min at 23°C, with detection by secondary antibodies and nuclear staining performed as described above. The position of Ad was evaluated compared to the positions of the MTOC and the nucleus.

Competence of Ad trafficking in enucleated cells over time after enucleation. Enucleated cells were prepared as described above. Following enucleation, cells were incubated for 0, 1, 3, 5, or 9 h prior to infection with Cy3-Ad by the method described above. The cells were then incubated for 60 min at 37°C. Following incubation, the cells were fixed and the MTOC and nuclei were stained as described above. The position of Ad was evaluated compared to the positions of the MTOC and nuclei.

Uniformity of Ad trafficking to the MTOC in enucleated cells. Enucleated cells were prepared and infected with carboxyfluorescein-Ad as described above. The

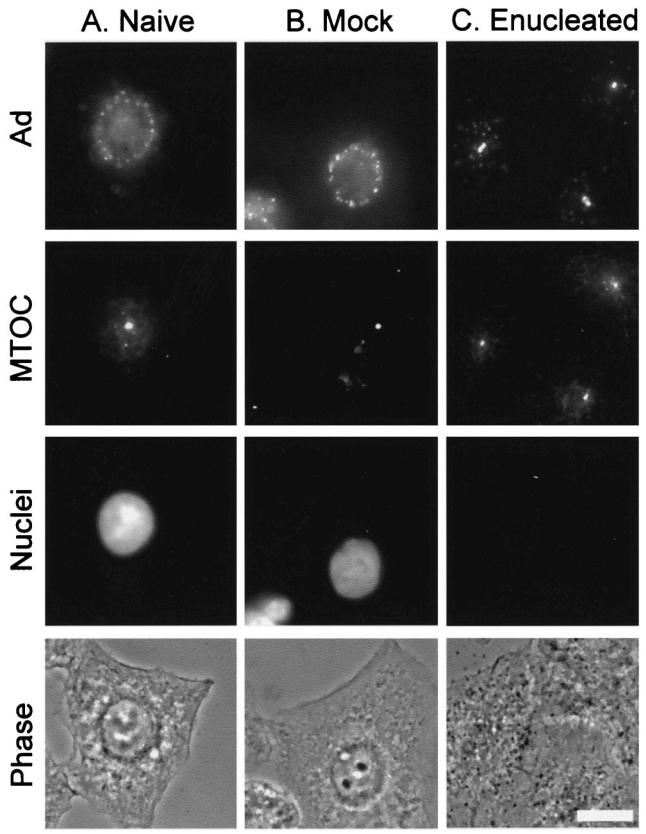

FIG. 3. Ad trafficking to the MTOC in the absence of a nucleus. Naive, mock-enucleated, and enucleated cells were prepared and infected as described for Fig. 2. Cells were incubated for 60 min following infection, and Cy3-Ad distribution was evaluated relative to nuclei (DAPI stain) and the MTOC (pericentrin staining). (A) Naive cells. (B) Mock-enucleated cells. (C) Enucleated cells. Each panel shows Cy3-Ad (Ad), pericentrin-staining (MTOC), DAPI-staining (nuclei), and phase-contrast (phase) images. Bar = 10 μm.

cells were then incubated for 0 or 60 min at 37°C. Following incubation, the cells were either fixed or reinfected with Cy3-Ad (10^{11} particles/ml, 10 min, 37°C) and then incubated for either 0 or 60 min at 37°C. Cells were fixed with methanol and the positions of carboxyfluorescein-Ad and Cy3-Ad were evaluated.

Capacity of Ad capsids to escape from endosomes in enucleated cells. Enucleated cells were infected with carboxyfluorescein-conjugated Ad (10^{11} particles per ml, 10 min, 37°C), washed, and incubated for an additional 60 min. In parallel, enucleated cells were treated with fluorescein-conjugated dextran (10,000 Da; Molecular Probes) at 5 mg/ml for 30 min, washed, and incubated for 60 min. Images of single microscopic fields of living cells were collected as follows: (i) initial image in binding buffer, (ii) second image in binding buffer, and (iii) third image in binding buffer supplemented with 50 mM methylamine, pH 7.0. Fluorescence intensity of the fluorescein probes was isolated by correcting for variations in the background fluorescence of the field by use of the "flatten background" algorithm in the MetaMorph image analysis software followed by digital background subtraction. In the processed image, a threshold intensity was set so that all fluorescence intensities exceeding 1% of the dynamic range of the camera would be integrated. Four fields of cells were quantified for each condition.

Ultrastructural analysis of the terminal localization of Ad in cells lacking a nucleus. Infected cells were analyzed by electron microscopy. Cells were infected with AdNull at 10^{11} particles/ml for 15 min at 37°C. Following infection, cells were either collected and fixed or incubated for 60 min prior to harvesting and fixation. Cells were washed three times with PBS containing 10 mM EGTA at 37°C, digested with trypsin, pelleted at 500 rpm (Beckman GH3.8 rotor) for 3 min, washed again with PBS-EGTA, and then fixed. Cells were fixed with 4% paraformaldehyde–2.5% glutaraldehyde–0.02% picric acid in 0.1 M sodium cacodylate buffer for 30 min. Samples were postfixed with 1% OsO_4–1.5% potassium ferricyanide in sodium cacodylate buffer, block stained with 1.5% aqueous uranyl acetate, dehydrated in graded alcohols, and embedded in EMbed 812 (Electron Microscopy Sciences). Ultrathin 60-nm sections were prepared and stained with uranyl acetate and lead citrate prior to examination with a JEOL 100CX-II transmission electron microscope.

Cy3-Ad and MTOC localization following treatment with cytochalasin B or nocodazole. Cells were either mock enucleated or enucleated and infected with Cy3-Ad as described above. Following the 60-min postinfection incubation, cells received no treatment (naive) or were treated with either dimethyl sulfoxide (DMSO) (0.1%, diluent control) (Sigma), cytochalasin B (20 μM, to depolymerize the actin microfilaments), or nocodazole (25 μM, to depolymerize the microtubules) for 20 min. Following drug treatment, the cells were fixed with methanol. The MTOC and nuclei were stained as described above, and the position of Ad was evaluated compared to those of the MTOC and nucleus.

Photobleaching analysis of stability of carboxyfluorescein-Ad association with the nuclei or MTOC. Mock-enucleated and enucleated cells were prepared as described above. Cells were either loaded with CellTracker Green fluorescent dye (5 μM, 60 min, 37°C) (Molecular Probes) or were infected with carboxyfluorescein-Ad and incubated for 60 min at 37°C. Following incubation, regions of cells were photobleached and imaged. A Zeiss LSM510 laser scanning confocal microscope running Zeiss software version 2.8 with a 25 mW argon laser operated at 75% output at 488 nm was used for bleaching (Zeiss, Thornwood, N.Y.). Cells were imaged by use of a ×63 N.A. 1.4 PlanApo DIC oil immersion objective lens, an HFT488 dichroic mirror, and an LP505 emission filter. A 96-μm-diameter pinhole allowed a 0.7-μm optical slice. The dwell time per pixel was 2.24 μs. The full frame was 512 by 512 pixels. Images were collected in z stacks with a step size of 0.5 or 0.6 μm. The initial image of the selected field was acquired by using 4% transmittance of the laser, with the photomultiplier tube optimized for 8-bit imaging. Selected regions were photobleached by 90 or 180 iterations of the 488-nm laser line at 100% transmittance. An image was recorded by using 4% laser transmittance immediately after completion of photobleaching. A 20-min recovery period was allowed and another image was collected. All imaging and the 20-min recovery period were done at room temperature. Analysis of the fluorescence intensities at the site of photobleaching was performed on images acquired prior to photobleaching, immediately following photobleaching, or following a 20-min incubation after photobleaching with the aid of Metamorph imaging software (Universal Imaging).

Long-term stability of Cy3-Ad association with the MTOC in cells lacking a nucleus. Mock-enucleated and enucleated cells were prepared and infected with Cy3-Ad as described above. Cells were then incubated for 0, 1, 3, 5, or 9 h at 37°C. Following incubation, cells were fixed with methanol and the MTOC and nuclei were stained as described above. Cy3-Ad distribution was evaluated relative to the MTOC and nuclei.

Statistical evaluation. Data are presented as means ± standard errors of the means. Statistical evaluations were performed by using the two-tailed Student *t* test.

RESULTS

Preparation of enucleated cells. Enucleation of A549 cells was modified from previously published methods (9, 33) in which cytochalasin B, a fungal metabolite known to depolymerize actin microfilaments, was added to cells to reduce cytoplasmic viscosity and cytoskeletal support for the plasma membrane. The weakened cells were then centrifuged to remove nuclei. Under the conditions described in Materials and Methods, <20% of cells detached from the monolayer. Of the remaining adherent cells, >95% were enucleated. The absence of nuclei was apparent by phase-contrast microscopy and was confirmed by use of the nucleic acid stain DAPI. The enucleated cells varied in morphology, ranging from broadly spread cells to partially retracted cells. All enucleated cells retained polymerized microtubules and intact intermediate filament cytoskeletal elements, as demonstrated by indirect immunofluorescence staining for tubulin, vimentin, actin, and cytokeratin (data not shown). To evaluate mitochondrial activity in enucleated cells, we stained the cultures with MitoTracker Red, a

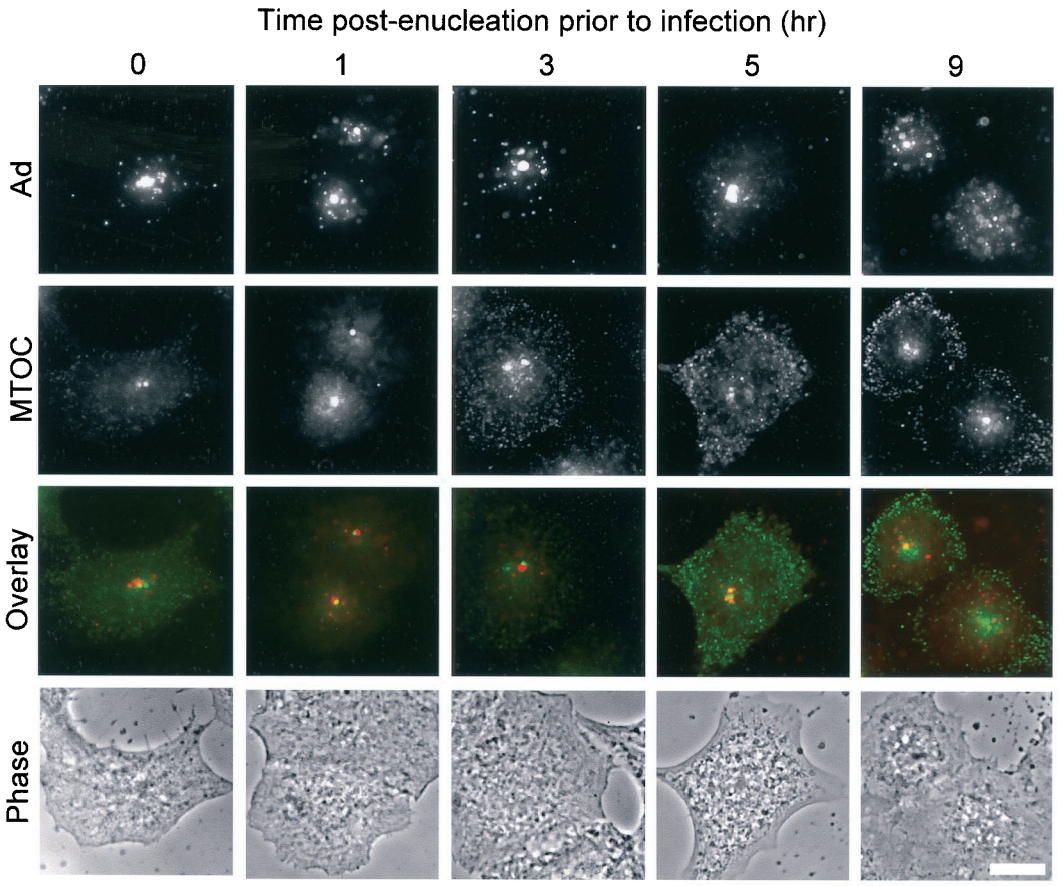

FIG. 4. Ad trafficking in enucleated cells over time. Enucleated cells were prepared as described for Fig. 2, washed, and incubated for 0 to 9 h prior to infection. Cells were then infected with Cy3-Ad, fixed, stained, and evaluated as for Fig. 3. Shown for the various times postenucleation and prior to infection are Cy3-Ad (red), MTOC (green), colocalization (yellow) (overlay), and phase-contrast (phase) images. Bar = 10 μm.

fluorescent dye which accumulates in metabolically active mitochondria. MitoTracker Red stained the mitochondria of naive and mock-enucleated A549 cells brightly but failed to stain the mitochondria of cells treated with sodium azide. Mitochondria in enucleated cells retained the ability to concentrate MitoTracker Red for at least 9 h after enucleation, which is indicative of continuing mitochondrial respiration over this time (data not shown).

The orientation of the monolayer relative to the direction of centrifugal *g* force was critical for efficient enucleation, with more rapid and gentler enucleation and less cell loss favored as the plane of the cell monolayer was brought perpendicular to the centrifugal force. Enucleation was equally effective whether we used cytochalasin B or a closely related compound, cytochalasin D. Use of either latrunculin A or latrunculin B, potent fungal toxins that cause disruption of microfilaments, resulted in unacceptably high levels of cell loss from the monolayer. Similarly, use of the microtubule depolymerizing agent, nocodazole, alone or in combination with any of the filamentous actin depolymerizing agents, resulted in excessive loss of cells from the monolayer. Centrifugation conditions were also variables in the process of enucleation. Centrifuge speeds of $>7{,}500 \times g$ as well as centrifuge times of >75 min increased loss of cells from the monolayer, while centrifuge speeds of $<6{,}500 \times g$ or centrifuge times of <55 min resulted in inefficient enucleation. The final centrifuge conditions optimized for enucleation of A549 cells were $7{,}250 \times g$ for 65 min. The temperature at which cells were centrifuged during enucleation also had an effect on the success of the technique. Enucleation was not possible at temperatures below 24°C and was highly inefficient (<50%) at temperatures below 34°C.

Ad trafficking in enucleated cells. To examine Ad trafficking, we performed all studies in naive A549 cells, mock-enucleated cells (cells centrifuged without the addition of cytochalasin B), and enucleated cells. To create a wave of viral infection that could be followed through the cells, we applied a high concentration of fluorophore-conjugated Ad to cells for a brief infection period and allowed the virus to traffic within cells for either 0 or 60 min. Immediately after infection, Cy3-Ad was localized to the cell periphery of naive, mock-enucleated, and enucleated cells (Fig. 2A to C). In naive and mock-enucleated cells, the virus trafficked to the nuclear envelope within 60 min (Fig. 2D and E). In enucleated cells, Cy3-Ad trafficked to the interior of enucleated cells within 60 min and was found in a discrete focus in the center of the cells (Fig. 2F). Prior to attaining focused intracellular localization in enucleated cells, Ad capsids were observed undergoing rapid, curvilinear translocation, which was previously attributed to microtubule-de-

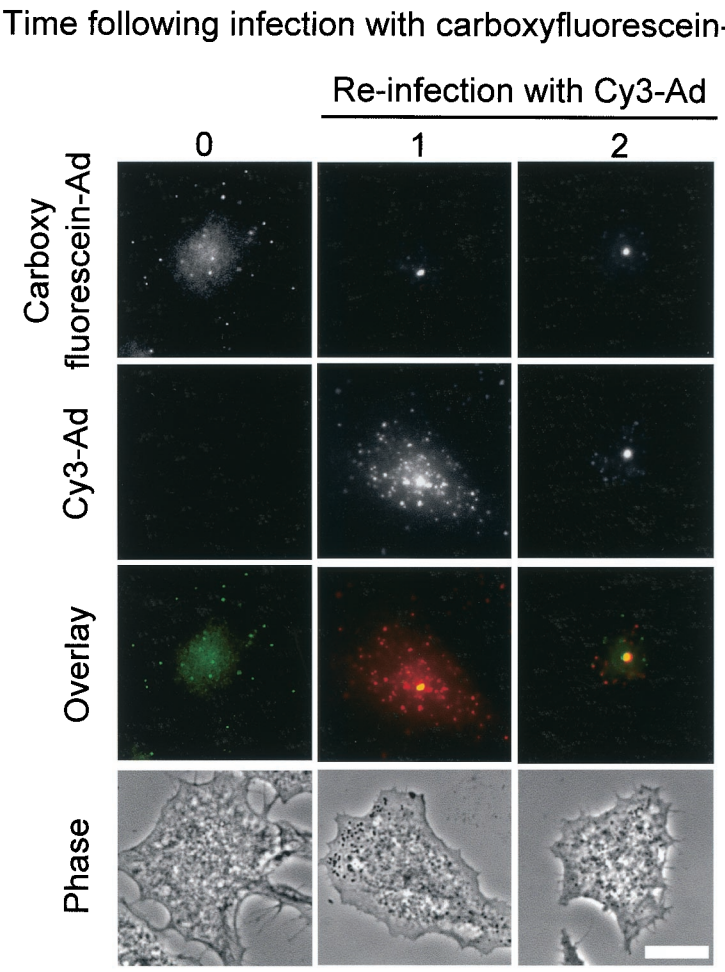

FIG. 5. Uniformity of trafficking pattern to the MTOC in enucleated cells. Enucleated cells were prepared and infected as for Fig. 2. Following infection with carboxyfluorescein-Ad (green), enucleated cells were incubated for 1 h and then reinfected with Cy3-labeled Ad (red). The reinfected enucleated cells were then incubated for 0 or 60 min. Colocalization of the two different Ads is indicated in yellow in the overlay of images. Bar = 10 μm.

pendent translocation (21, 22, 43). When Ad was translocating, mean velocities in excess of 2 μm/s (2.2 ± 0.1 μm/s for mock-enucleated cells and 2.4 ± 0.2 μm/s for enucleated cells [n = 50 for each group; $P > 0.05$]) were observed in both mock-enucleated and enucleated cells, indicative of microtubule-dependent trafficking.

Given prior observations that Ad traffics along microtubules, the MTOC was hypothesized to be the site of Ad accumulation in enucleated cells. This hypothesis was tested by staining the cells with an antibody against pericentrin, a major component of the MTOC. Indirect immunofluorescence staining of pericentrin revealed one or two discrete pericentrin-positive structures per cell located in close proximity to the nucleus. In naive and mock-enucleated A549 cells, Cy3-Ad was found associated with the nuclear envelope 60 min after infection (Fig. 3A and B). In naive or mock-enucleated A549 cells, there was no preferential localization of Ad to the MTOC. In enucleated cells, nearly perfect colocalization was observed between the pericentrin-stained MTOC and the discrete focus of Cy3-Ad in enucleated A549 cells 1 h after infection (Fig. 3C). Enucleated cells were competent to internalize Cy3-Ad and allowed trafficking to the MTOC for at least 5 h after enucleation (Fig. 4). At 9 h postenucleation, the localization at the MTOC was reduced and the structure of the MTOC appeared to be dispersed in some cells.

We further examined the uniformity of Ad capsid trafficking to the MTOC by reinfecting the enucleated cells with a second fluorophore-labeled virus. Enucleated A549 cells were infected with carboxyfluorescein-Ad and incubated for 60 min to allow the Ad to traffic to the MTOC. The culture then received a second infection with Cy3-conjugated Ad, which fluoresces in the red channel. Cells that were fixed immediately after the second infection revealed a peripheral staining pattern of Cy3-Ad which did not colocalize with the centrally located carboxyfluorescein-Ad (Fig. 5). When an incubation period of 60 min was added to allow Cy3-Ad to traffic within the enucleated cells, Cy3-Ad was found colocalized with carboxyfluorescein-Ad, indicating that Ad capsids infecting enucleated cells at different times trafficked to a uniform intracellular structure, consistent with MTOC localization (Fig. 5).

Cytosolic localization of Ad in enucleated cells. To ensure that there was no defect in the escape of Ad from endosomes

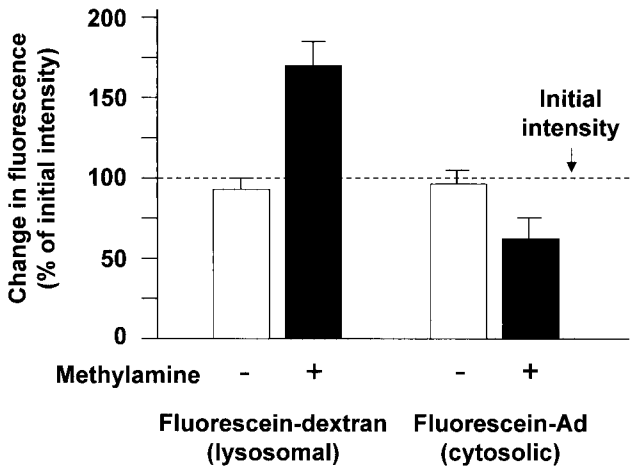

FIG. 6. Ad capsid escape from endosomes in enucleated cells. Enucleated A549 cells were incubated with either fluorescein-dextran or carboxyfluorescein-Ad followed by a 1-h incubation. The fluorescein fluorescence intensity was measured in living cells in the absence or presence of methylamine (pH 7.0) and compared to the fluorescence intensity of an initial image that was acquired in the absence of methylamine (dashed line). Fluorescein-dextran, a marker of lysosomes, showed a 71% increase in fluorescence intensity following the addition of methylamine, indicating localization in an acidic compartment. Carboxyfluorescein-Ad fluorescence intensity did not increase following the addition of methylamine, indicating localization in a neutral compartment, consistent with cytosolic localization.

in enucleated cells and that the interaction of Ad with the MTOC in enucleated cells resulted from the direct interaction of capsid with cytoskeleton, we performed fluorescence and ultrastructural studies to evaluate the cytosolic localization of Ad following infection of enucleated cells. First, the escape of Ad from endosomes was tested based on the fact that acidic pH quenches the fluorescence intensity of fluorescein. Neutralization of acidic endosomes leads to an increase in fluorescein fluorescence intensity, whereas no increase in fluorescence intensity is observed when fluorescein is located in the cytosol, which maintains neutral pH. Neutralization of endosomes was accomplished by the addition of the weak base methylamine, buffered to pH 7.0 (25). As a control, fluorescein-conjugated dextran was loaded into cells by bulk fluid phase uptake and was allowed to traffic to lysosomes with a 60-min incubation. Sequential images of a single field of enucleated cells in the absence of methylamine resulted in a similar fluorescence intensity in the second image compared to that in the initial image (Fig. 6). However, the addition of methylamine resulted in an increase in fluorescence intensity of 71 ± 13% ($P < 0.001$, compared to the absence of methylamine), demonstrating that the fluorescein-dextran was located within an acidic compartment. Carboxyfluorescein exhibits the same pH-dependent quenching as fluorescein, and carboxyfluorescein-Ad was analyzed in the same manner. As observed for dextran, sequential images of a single field of carboxyfluorescein-Ad-infected enucleated cells in the absence of methylamine resulted in a similar fluorescence intensity in the second image compared to that in the initial image. In contrast to the result seen for fluorescein-dextran, the addition of methylamine resulted in a modest decrease in fluorescence intensity of 34 ± 10% ($P < 0.02$, compared to the absence of methylamine), which was likely due to photobleaching. The failure of methylamine to increase the fluorescence intensity of carboxyfluorescein-Ad demonstrated that the population of Ad was located within a neutral compartment, likely the cytosol of the enucleated cell.

This hypothesis was directly tested by electron microscopy. Ultrathin sections of cells infected with Ad for 15 min showed virus at the cell surface, in endosomes, and free in the cytosol (Fig. 7A). In mock-enucleated cells, Ad trafficked to the nuclear envelope, where intact Ad capsids were observed 60 min after infection (Fig. 7B). Uncoated Ad capsids were also recognized at the nuclear envelope based on their size (75 nm)

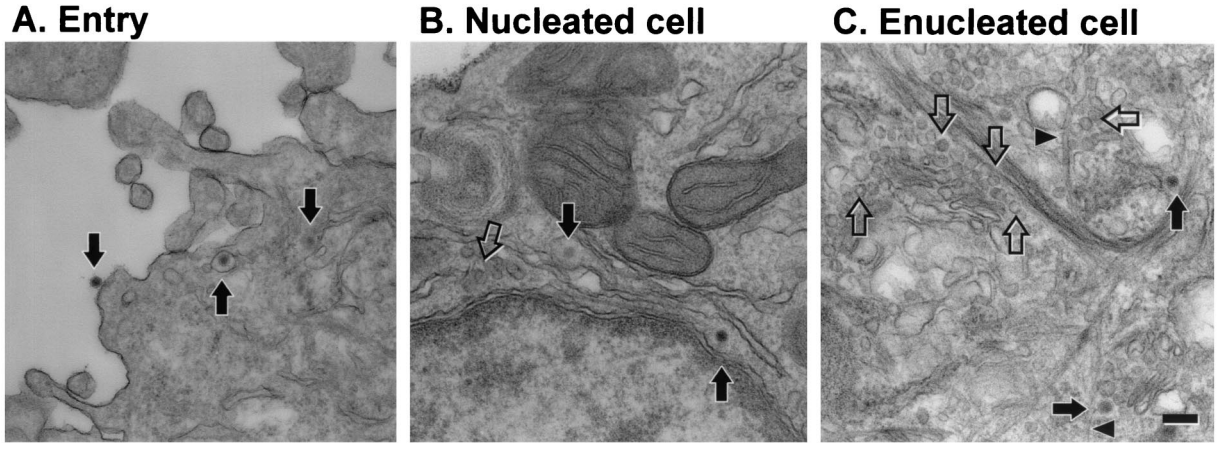

FIG. 7. Ultrastructural localization of Ad in mock-enucleated and enucleated cells. Mock-enucleated and enucleated cells were prepared as for Fig. 2. Cells were infected for 15 min with AdNull, washed, and fixed or incubated for 60 min at 37°C prior to fixation. (A) Entry of Ad into cells after a 15-min infection. Ad capsids are visible at the cell surface, in an endosome, and free in the cytosol (arrows, left to right). (B) Mock-enucleated cell at 60 min postinfection. Both intact Ad capsids (filled arrows) and empty Ad capsids (open arrow) are located near the nuclear envelope. (C) Enucleated cell at 60 min postinfection. Both intact Ad capsids (filled arrows) and empty Ad capsids (open arrows) are located near the center of the enucleated cell. Some Ad capsids are located adjacent to microtubules (arrowheads). Well-organized centrioles were not observed in enucleated, mock-enucleated, or naive A549 cells. Bar = 200 nm.

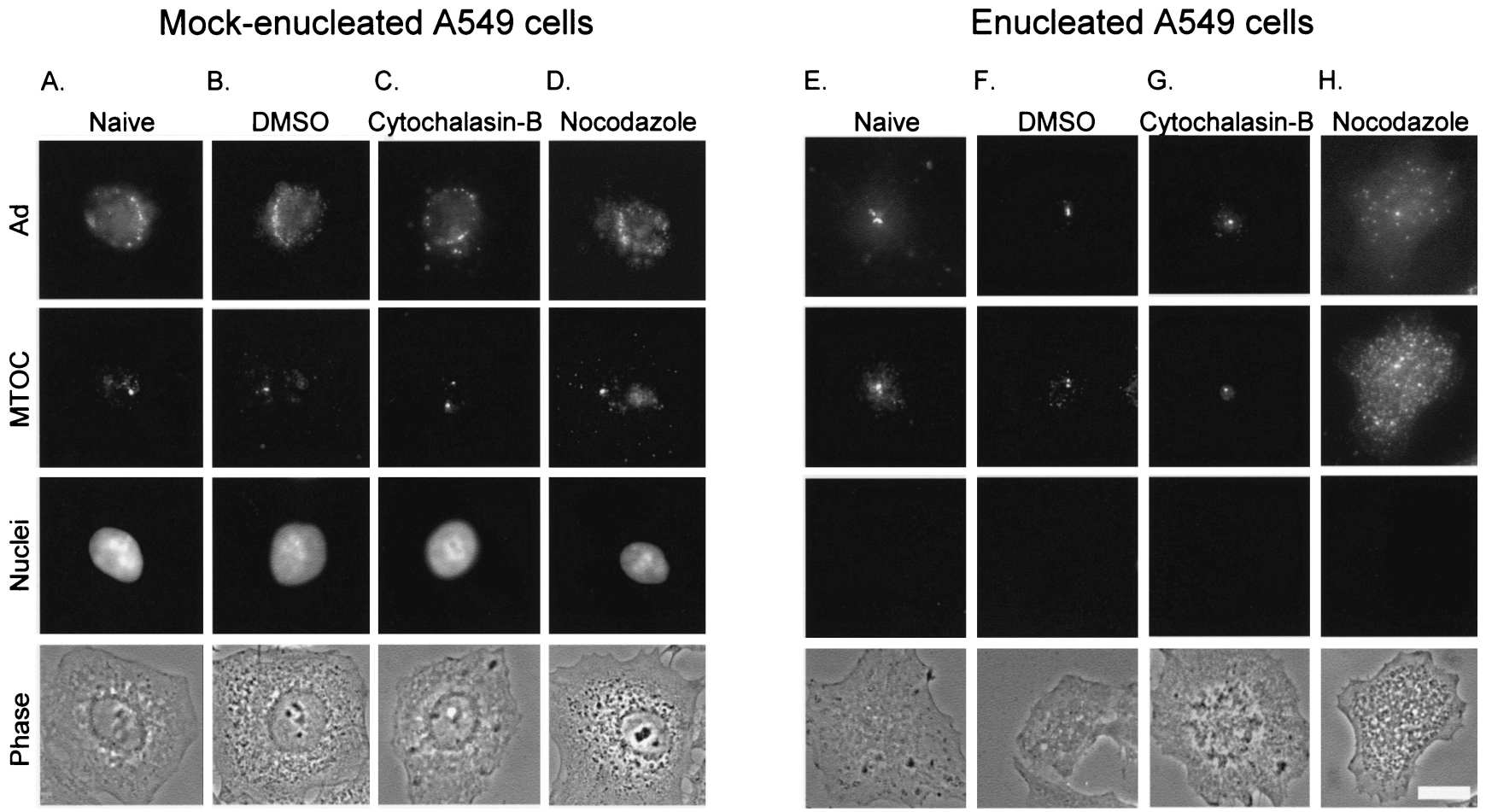

FIG. 8. Effect of microtubule disruption on Ad and MTOC localization. Cells were enucleated and infected as for Fig. 2. Following the 1-h postinfection incubation, mock-enucleated or enucleated cells were left untreated (naive) or were treated with either DMSO, cytochalasin B, or nocodazole for 20 min. The cells were then fixed, and the MTOC and nuclei were stained as for Fig. 3. Shown for each treatment are Cy3-Ad (Ad), pericentrin-stained (MTOC), DAPI-stained (nuclei), and phase-contrast (phase) images. (A) Naive mock-enucleated cells. (B) Mock-enucleated cells treated with DMSO. (C) Mock-enucleated cells treated with cytochalasin B. (D) Mock-enucleated cells treated with nocodazole. (E) Naive enucleated cells. (F) Enucleated cells treated with DMSO. (G) Enucleated cells treated with cytochalasin B. (H) Enucleated cells treated with nocodazole. Bar = 10 μm.

and the clearly angular nature of their profiles (Fig. 7B). In enucleated cells, collections of intact and uncoated Ad capsids were found near the center of the cytosol (Fig. 7C). Individual microtubules as well as bundles of intermediate filaments were readily apparent. However, intact centrioles were not clearly discernible in either enucleated, mock-enucleated, or naive A549 cells despite the presence of a well-organized focus of pericentrin (Fig. 3, 4, and 5). Electron microscopy and evaluation of the neutral environment of Ad vectors clearly demonstrate the direct access of Ad capsids to the cytoskeleton in enucleated cells.

Localization of Cy3-Ad following cytoskeletal perturbation. Based on the morphological colocalization of Cy3-Ad and pericentrin described above, we hypothesized that Cy3-Ad was bound to the MTOC in enucleated cells. To confirm this hypothesis, we tested the stability of Cy3-Ad localization in the presence of a microtubule-depolymerizing agent, nocodazole. One hour after infection of mock-enucleated and enucleated cells with fluorophore-labeled Ad, cell cultures were treated with cytoskeleton-perturbing agents. The localization of Cy3-Ad following infection was compared in naive cells and in cells that were treated with DMSO (the diluent of the cytoskeleton-perturbing drugs), cytochalasin B (an actin microfilament-depolymerizing agent), and nocodazole (a microtubule-depolymerizing agent). Cy3-Ad was found associated with the nucleus in mock-enucleated naive cells, DMSO-treated cells, and cells treated with either cytochalasin B or nocodazole (Fig. 8A to D). Once the virus trafficked to the nuclear envelope, the association was maintained regardless of drug treatment. For mock-enucleated cells, the pericentrin-stained MTOC was unaltered in naive cells, DMSO-treated cells, and cytochalasin B-treated cells (Fig. 8A to C); however, the pericentrin distribution was disrupted upon treatment with nocodazole (Fig. 8D). In the naive enucleated cells, the virus trafficked to the MTOC (Fig. 8E). The association was maintained in the presence of DMSO or cytochalasin B (Fig. 8F and G); however, the viral capsid distribution, like the pericentrin distribution, was disrupted upon treatment with nocodazole (Fig. 8H).

Stability of Cy3-Ad association with the MTOC in enucleated cells. As a test of the stability of the Ad-MTOC interaction, fluorescence recovery after photobleaching was employed. This approach tested for the ability of a population of fluorescent molecules to reestablish an equilibrium distribution after one part of the population was photobleached with a laser. For this experiment, rapid fluorescence recovery indicated a mobile fluorophore whereas slow fluorescence recovery indicated a static fluorophore. Given the ability of Ad to move along microtubules at rates up to 2 μm/s and the relatively short distance required for redistribution to occur (<2 μm between adjacent areas of nuclear envelope or adjacent MTOCs), a recovery time of 20 min following photobleaching was chosen. As a positive control for photobleaching and fluorescence recovery after photobleaching, mock-enucleated cells were loaded with CellTracker Green dye and then imaged and photobleached (Fig. 9A). For evaluation of the mobility of carboxyfluorescein-Ad at the nuclear envelope of mock-enucleated cells or at the MTOC of enucleated cells, the carboxyfluorescein signal was imaged and photobleached (Fig. 9B and C). At the site of bleaching, the intensity of the fluorophore signal was measured in images taken immediately after photobleaching and again after a 20-min recovery period. The mock-enucleated cells loaded with CellTracker Green dye had only 41% fluorescence intensity remaining in the bleached region immediately following bleaching but recovered to 80%

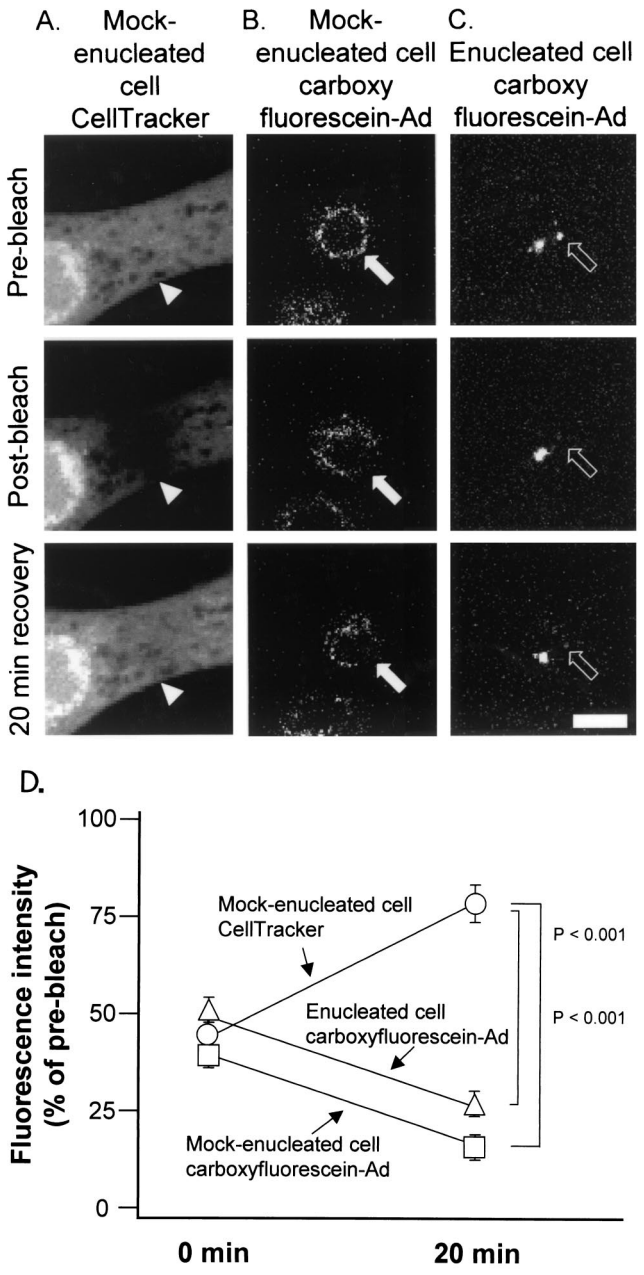

FIG. 9. Short-term stability of Cy3-Ad association with the MTOC in cells lacking a nucleus. Mock-enucleated and enucleated cells were prepared as for Fig. 2. Cells were either loaded with CellTracker Green fluorescent dye or infected for 10 min with carboxyfluorescein-Ad, washed, and incubated for 60 min at 37°C. Following incubation, regions of cells were photobleached with an argon laser at 488 nm. Images were collected with a confocal microscope before bleaching, after bleaching, and following a 20-min recovery period. (A) Mock-enucleated cell stained with CellTracker Green. (B) Mock-enucleated cell infected with carboxyfluorescein-Ad. (C) Enucleated cell infected with carboxyfluorescein-Ad. (D) Quantitative analysis of the fluorescence intensity at the site of bleaching. Bar = 10 μm.

of the initial cellular fluorescence during the 20-min recovery period (Fig. 9D). The carboxyfluorescein-Ad signal in both mock-enucleated and enucleated cells was bleached to a fluorescence intensity equal to 36 or 49% of the initial total fluorescence intensity, respectively. Carboxyfluorescein-Ad associated with the nuclear envelope did not redistribute from other areas of the nucleus to the bleached area, and carboxyfluorescein-Ad associated with one MTOC did not redistribute to the bleached MTOC (Fig. 9D). The data demonstrate a lack of fluorescence recovery after photobleaching, consistent with the failure of Ad to dissociate from the nuclear envelope or MTOC and traffic to the adjacent area of the nuclear envelope or adjacent MTOC, respectively. The stability of the association between Ad and the MTOC was further probed by analyzing the kinetics of Ad arrival at the MTOC compared with Ad departure from the MTOC. For comparison, arrival and departure kinetics were also determined for Ad association with the nucleus. Ad showed a strong bias toward associating with nuclei in mock-enucleated cells or the MTOC in enucleated cells and infrequently was observed to dissociate from either complex (Table 1).

Long-term stability of Cy3-Ad association with the MTOC in cells lacking nuclei. Ad trafficked to the nucleus in mock-enucleated cells and remained bound to the nucleus for at least 5 h postinfection and to a high degree, though with some dissociation, up to 9 h postinfection (Fig. 10A). Ad trafficked to the MTOC in enucleated cells and remained associated with the MTOC structure for at least 5 h postinfection (Fig. 10B). In enucleated cells that were infected with Cy3-Ad and incubated for 9 h postinfection, Ad capsids remained associated with the MTOC to some extent. However, much of the viral capsid became dissociated at this late time point (Fig. 10B). Additionally, many cells exhibited dissociation and dispersion of Ad and pericentrin (Fig. 10B).

DISCUSSION

The present study of the infection pathway of Ad is relevant to the transition from microtubule-mediated translocation to initiation of binding to the nuclear envelope. To examine the process of dissociation of Ad from the microtubule cytoskeleton, a system was developed to characterize Ad infection in cells lacking nuclei. In these enucleated cells, Ad was observed to traffic to a discrete, postendosomal, intracellular location that colocalized with pericentrin, a marker of the MTOC. The MTOC localization was confirmed by studies showing that the microtubule-depolymerizing agent nocodazole induced a redistribution of Ad throughout the cell. The association of Ad with the MTOC was surprisingly stable, with the association maintained for up to 9 h after infection, a time course that matched the extent of Ad association with the nuclear envelope in mock-enucleated cells. Examination of the arrival and departure frequencies of Ad at the MTOC revealed that the net movement of Ad heavily favored arrival at the MTOC rather than departure from the MTOC. An analogous study in mock-enucleated cells showed a similar preference for binding over dissociation from the nuclear envelope, indicating that the affinities of the MTOC and nuclear envelope for Ad capsid were comparable. Finally, fluorescence recovery after photobleaching showed that the population of MTOC-associated Ad was not capable of redistribution by microtubule-mediated translocation from one MTOC to another, just as nuclear envelope-associated Ad was not capable of redistributing by microtubule-mediated translocation from a nonbleached area of the nuclear envelope to fill the bleached area of the nuclear envelope. Together, the three different means of assessment (long-term incubation, frequency of Ad arrival versus departure, and analysis of fluorescence recovery after photobleaching) all support the conclusion that the association of Ad with the MTOC in enucleated cells is stable and is comparable to the stability of Ad association with the nuclear envelope in mock-enucleated cells.

The observation of a stable association of Ad with the MTOC in the absence of a nucleus has important implications for the understanding of the late stages of Ad infection. Ultimately, Ad binds to the nuclear envelope near the site of nuclear pores, where both DNA-containing and empty Ad capsids have been observed at the nuclear envelope (7, 10). As infection progresses, the proportion of empty Ad capsids increases, leading to the model that Ad arrives at the nuclear envelope prior to release of DNA from the capsid (7, 10). One possibility is that the Ad capsid has a higher affinity for the nuclear envelope than for any other structure in the cytosol. Binding of Ad to the nuclear envelope has been observed by use of purified components in vitro (38, 47, 51). In this nuclear envelope affinity sink model for nuclear localization, Ad capsids will eventually develop an association with the nuclear envelope by an iterative process, establishing and then disengaging from less stable associations with other cytosolic structures such as microtubules. The observation presented here that the Ad-MTOC association is highly stable can only be consistent with the nuclear envelope affinity sink model if the Ad capsid rarely forms a highly stable association with the MTOC during infection of a normal cell. This result could occur if the organization of the microtubule cytoskeleton makes it likely that Ad will encounter the nucleus prior to reaching the MTOC. In this scenario, a microtubule cytoskeleton composed of highly curved microtubules may be more likely to deliver Ad to the nucleus prior to encountering the MTOC, whereas a microtubule cytoskeleton composed of simple straight microtubules such as that found in fibroblasts may be more likely to deliver Ad to the MTOC first. Alternatively, the stability of the Ad-MTOC interaction suggests that an "MTOC rescue" model might be invoked. Some cellular activity, either at the MTOC or associated with the nuclear envelope, could mediate active release of Ad from microtubules to the nuclear envelope. Candidates for this activity include cytosolic proteins, such as those involved in proteasome-mediated degradation found at the MTOC in structures named aggresomes (20). An aggresome is a transient entity that forms in response to misfolded proteins. It is possible that the cell recognizes the Ad capsid as a misfolded protein, stimulating formation of an aggresome at the MTOC. This hypothesis is consistent with the observation of aggresome formation induced by other viral antigens (1). It is known that unfolding of proteins prior to proteasomal degradation requires the functioning of cytosolic molecular chaperones, including the family of heat shock proteins (18). Several heat shock proteins have been implicated in the Ad infection pathway, although the functions of these proteins have not yet been determined (31,

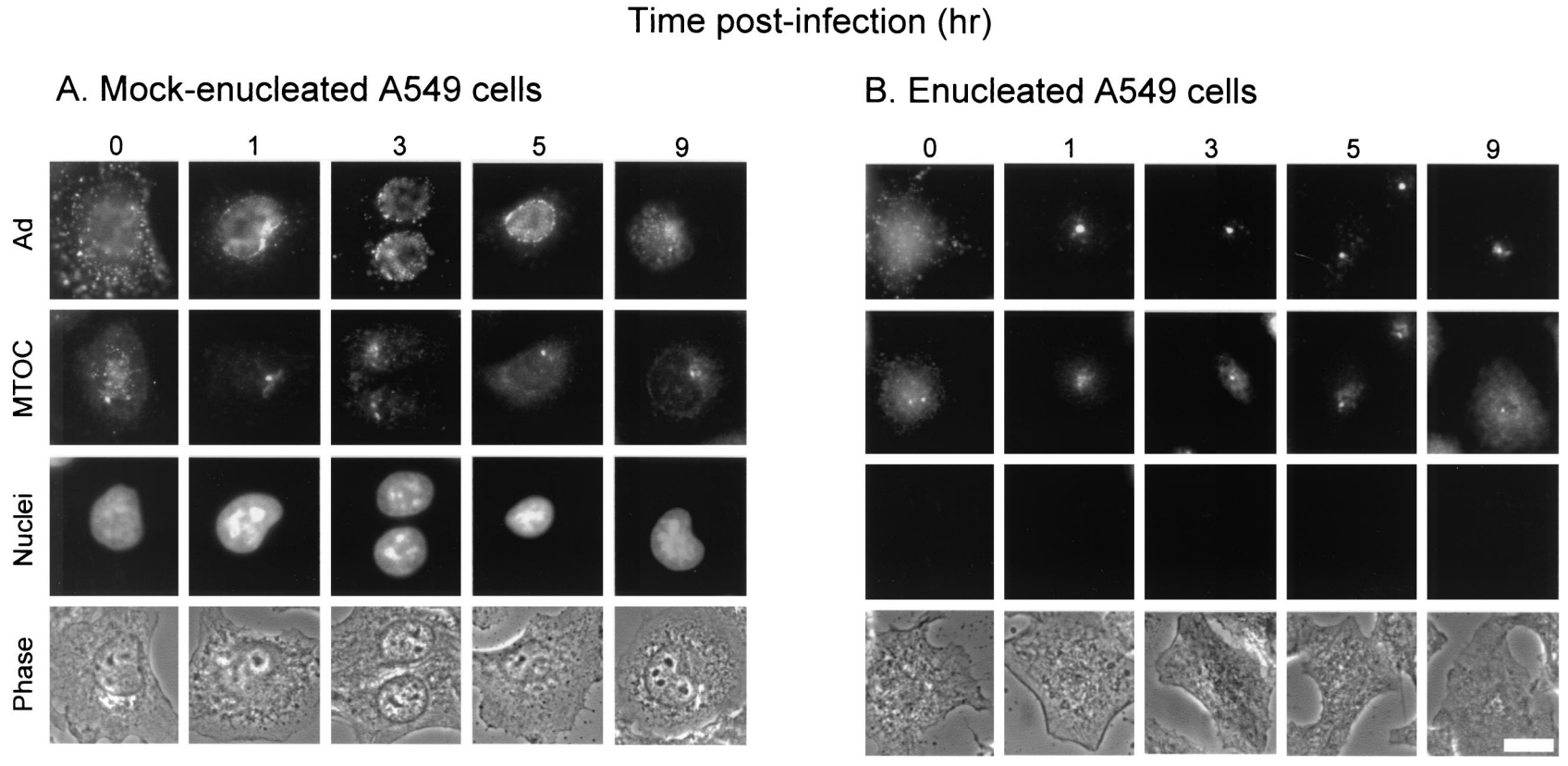

FIG. 10. Long-term stability of Cy3-Ad association with the MTOC in cells lacking a nucleus. Mock-enucleated and enucleated cells were prepared as for Fig. 2. Cells were infected for 10 min with Cy3-Ad, washed, and incubated for 0 to 9 h at 37°C. Cy3-Ad distribution was evaluated relative to nuclei (DAPI stain) and the MTOC (pericentrin staining). The length of time of incubation of cells following the addition of Cy3-Ad is shown at the top. (A) Mock-enucleated cells. (B) Enucleated cells. Bar = 10 μm.

TABLE 1. Arrival and departure of Ad from terminal trafficking locations

Condition	Terminal location	Trafficking pattern (events/min [*n*]) of Ad at indicated times postinfection[a]					
		40 to 60 min			60 to 90 min		
		Arrival	Departure	*P*	Arrival	Departure	*P*
Mock-enucleated cells	Nuclear envelope	35.4 ± 2.5 (531)	2.6 ± 0.3 (39)	<0.001	25.2 ± 1.6 (378)	1.4 ± 0.3 (21)	<0.001
Enucleated cells	MTOC	45.7 ± 1.1 (686)	3.2 ± 0.3 (48)	<0.001	15.2 ± 1.4 (228)	1.6 ± 0.4 (24)	<0.001

[a] Data are means ± standard errors of the means.

38). Interestingly, our observation that two distinct waves of viral infection could achieve MTOC localization to the same structure suggests that the cellular components that maintain the Ad-MTOC association were not limiting under our conditions. The MTOC rescue model and nuclear affinity sink models are not mutually exclusive, and some combination of these models may result in the final association of Ad with the nuclear envelope.

Other than Ad, many other viruses require microtubule-mediated translocation as part of their infection pathway. The herpesvirus nucleocapsid, like that of Ad, requires the activity of the microtubule-associated molecular motor cytoplasmic dynein to achieve nuclear localization (12). Microtubule-dependent motility appears to be a broadly utilized mechanism by which the efficiency of viral infection is enhanced (3, 41). The principle of stable association of viral capsid with the MTOC documented here may play a role in our understanding of the infection pathway of other viruses as well. Enucleated cells have been used previously as model systems to study the nuclear dependence of viral replication (34). The present research demonstrates the utility of enucleated cells for studying intracellular trafficking pathways during viral infection.

ACKNOWLEDGMENTS

We thank Lee Cohen-Gould (Optical and Electron Microscopy Core Facilities) for assistance with confocal microscopy and electron microscopy and N. Mohamed and T. Virgin-Bryan for help in preparing the manuscript.

These studies were supported in part by grants P01 HL51746, P01 HL59312, and R01 AR46282-01A1; the Will Rogers Memorial Fund, Los Angeles, Calif.; and GenVec, Inc., Gaithersburg, Md. C.J.B. was supported in part by NIH grant T32 HL07423.

REFERENCES

1. **Antón, L. C., U. Schubert, I. Bacik, M. F. Princiotta, P. A. Wearsch, J. Gibbs, P. M. Day, C. Realini, M. C. Rechsteiner, J. R. Bennink, and J. W. Yewdell.** 1999. Intracellular localization of proteasomal degradation of a viral antigen. J. Cell Biol. **146:**113–124.
2. **Bai, M., B. Harfe, and P. Freimuth.** 1993. Mutations that alter an Arg-Gly-Asp (RGD) sequence in the adenovirus type 2 penton base protein abolish its cell-rounding activity and delay virus reproduction in flat cells. J. Virol. **67:**5198–5205.
3. **Bearer, E. L., and P. Satpute-Krishnan.** 2002. The role of the cytoskeleton in the life cycle of viruses and intracellular bacteria: tracks, motors, and polymerization machines. Curr. Drug Targets Infect. Disord. **2:**247–264.
4. **Bergelson, J. M., J. A. Cunningham, G. Droguett, E. A. Kurt-Jones, A. Krithivas, J. S. Hong, M. S. Horwitz, R. L. Crowell, and R. W. Finberg.** 1997. Isolation of a common receptor for coxsackie B viruses and adenoviruses 2 and 5. Science **275:**1320–1323.
5. **Bornens, M.** 2002. Centrosome composition and microtubule anchoring mechanisms. Curr. Opin. Cell Biol. **14:**25–34.
6. **Chardonnet, Y., and S. Dales.** 1970. Early events in the interaction of adenoviruses with HeLa cells. I. Penetration of type 5 and intracellular release of the DNA genome. Virology **40:**462–477.
7. **Chardonnet, Y., and S. Dales.** 1972. Early events in the interaction of adenoviruses with HeLa cells. III. Relationship between an ATPase activity in nuclear envelopes and transfer of core material: a hypothesis. Virology **48:**342–359.
8. **Cooper, J. A.** 1987. Effects of cytochalasin and phalloidin on actin. J. Cell Biol. **105:**1473–1478.
9. **Crenshaw, A. H., J. W. Shay, and L. R. Murrell.** 1980. Mass enucleation of tissue culture cell monolayers. J. Tissue Culture Methods **6:**127–130.
10. **Dales, S., and Y. Chardonnet.** 1973. Early events in the interaction of adenoviruses with HeLa cells. IV. Association with microtubules and the nuclear pore complex during vectorial movement of the inoculum. Virology **56:**465–483.
11. **Davison, E., R. M. Diaz, I. R. Hart, G. Santis, and J. F. Marshall.** 1997. Integrin α5β1-mediated adenovirus infection is enhanced by the integrin-activating antibody TS2/16. J. Virol. **71:**6204–6207.
12. **Dohner, K., A. Wolfstein, U. Prank, C. Echeverri, D. Dujardin, R. Vallee, and B. Sodeik.** 2002. Function of dynein and dynactin in herpes simplex virus capsid transport. Mol. Biol. Cell **13:**2795–2809.
13. **Fitz Gerald, D. J., R. Padmanabhan, I. Pastan, and M. C. Willingham.** 1983. Adenovirus-induced release of epidermal growth factor and pseudomonas toxin into the cytosol of KB cells during receptor-mediated endocytosis. Cell **32:**607–617.
14. **Glotzer, J. B., A. I. Michou, A. Baker, M. Saltik, and M. Cotten.** 2001. Microtubule-independent motility and nuclear targeting of adenoviruses with fluorescently labeled genomes. J. Virol. **75:**2421–2434.
15. **Greber, U. F., M. Willetts, P. Webster, and A. Helenius.** 1993. Stepwise dismantling of adenovirus 2 during entry into cells. Cell **75:**477–486.
16. **Greber, U. F., M. Suomalainen, R. P. Stidwill, K. Boucke, M. W. Ebersold, and A. Helenius.** 1997. The role of the nuclear pore complex in adenovirus DNA entry. EMBO J. **16:**5998–6007.
17. **Hersh, J., R. G. Crystal, and B. Bewig.** 1995. Modulation of gene expression after replication-deficient, recombinant adenovirus-mediated gene transfer by the product of a second adenovirus vector. Gene Ther. **2:**124–131.
18. **Höhfeld, J., D. M. Cyr, and C. Patterson.** 2001. From the cradle to the grave: molecular chaperones that may choose between folding and degradation. EMBO Rep. **2:**885–890.
19. **Huang, S., T. Kamata, Y. Takada, Z. M. Ruggeri, and G. R. Nemerow.** 1996. Adenovirus interaction with distinct integrins mediates separate events in cell entry and gene delivery to hematopoietic cells. J. Virol. **70:**4502–4508.
20. **Kopito, R. R.** 2000. Aggresomes, inclusion bodies and protein aggregation. Trends Cell Biol. **10:**524–530.
21. **Leopold, P. L., B. Ferris, I. Grinberg, S. Worgall, N. R. Hackett, and R. G. Crystal.** 1998. Fluorescent virions: dynamic tracking of the pathway of adenoviral gene transfer vectors in living cells. Hum. Gene Ther. **9:**367–378.
22. **Leopold, P. L., G. Kreitzer, N. Miyazawa, S. Rempel, K. K. Pfister, E. Rodriguez-Boulan, and R. G. Crystal.** 2000. Dynein- and microtubule-mediated translocation of adenovirus serotype 5 occurs after endosomal lysis. Hum. Gene Ther. **11:**151–165.
23. **Luduena, R. F., and M. C. Roach.** 1991. Tubulin sulfhydryl groups as probes and targets for antimitotic and antimicrotubule agents. Pharmacol. Ther. **49:**133–152.
24. **Mabit, H., M. Y. Nakano, U. Prank, B. Saam, K. Dohner, B. Sodeik, and U. F. Greber.** 2002. Intact microtubules support adenovirus and herpes simplex virus infections. J. Virol. **76:**9962–9971.
25. **Maxfield, F. R.** 1982. Weak bases and ionophores rapidly and reversibly raise the pH of endocytic vesicles in cultured mouse fibroblasts. J. Cell Biol. **95:**676–681.
26. **Mitchison, T., and M. Kirschner.** 1984. Microtubule assembly nucleated by isolated centrosomes. Nature **312:**232–237.
27. **Mitchison, T., and M. Kirschner.** 1984. Dynamic instability of microtubule growth. Nature **312:**237–242.
28. **Mittereder, N., K. L. March, and B. C. Trapnell.** 1996. Evaluation of the concentration and bioactivity of adenovirus vectors for gene therapy. J. Virol. **70:**7498–7509.
29. **Miyazawa, N., P. L. Leopold, N. R. Hackett, B. Ferris, S. Worgall, E. Falck-Pedersen, and R. G. Crystal.** 1999. Fiber swap between adenovirus subgroups B and C alters intracellular trafficking of adenovirus gene transfer vectors. J. Virol. **73:**6056–6065.
30. **Nakano, M. Y., K. Boucke, M. Suomalainen, R. P. Stidwill, and U. F. Greber.** 2000. The first step of adenovirus type 2 disassembly occurs at the cell surface, independently of endocytosis and escape to the cytosol. J. Virol. **74:**7085–7095.

31. **Niewiarowska, J., J. D. D'Halluin, and M. T. Belin.** 1992. Adenovirus capsid proteins interact with HSP70 proteins after penetration in human or rodent cells. Exp. Cell Res. **201:**408–416.
32. **Prchla, E., C. Plank, E. Wagner, D. Blaas, and R. Fuchs.** 1995. Virus-mediated release of endosomal content in vitro: different behavior of adenovirus and rhinovirus serotype 2. J. Cell Biol. **131:**111–123.
33. **Prescott, D. M., D. Myerson, and J. Wallace.** 1972. Enucleation of mammalian cells with cytochalasin B. Exp. Cell Res. **71:**480–485.
34. **Pringle, C. R.** 1977. Enucleation as a technique in the study of virus interactions. Curr. Top. Microbiol. Immunol. **76:**49–82.
35. **Rosenfeld, M. A., W. Siegfried, K. Yoshimura, K. Yoneyama, M. Fukayama, L. E. Stier, P. K. Paakko, P. Gilardi, L. D. Stratford-Perricaudet, and M. Perricaudet.** 1991. Adenovirus-mediated transfer of a recombinant alpha 1-antitrypsin gene to the lung epithelium in vivo. Science **252:**431–434.
36. **Rosenfeld, M. A., K. Yoshimura, B. C. Trapnell, K. Yoneyama, E. R. Rosenthal, W. Dalemans, M. Fukayama, J. Bargon, L. E. Stier, and L. Stratford-Perricaudet.** 1992. In vivo transfer of the human cystic fibrosis transmembrane conductance regulator gene to the airway epithelium. Cell **68:**143–155.
37. **Salmon, E. D., R. J. Leslie, W. M. Saxton, M. L. Karow, and J. R. McIntosh.** 1984. Spindle microtubule dynamics in sea urchin embryos: analysis using a fluorescein-labeled tubulin and measurements of fluorescence redistribution after laser photobleaching. J. Cell Biol. **99:**2165–2174.
38. **Saphire, A. C., T. Guan, E. C. Schirmer, G. R. Nemerow, and L. Gerace.** 2000. Nuclear import of adenovirus DNA in vitro involves the nuclear protein import pathway and hsc70. J. Biol. Chem. **275:**4298–4304.
39. **Shenk, T. E.** 2001. *Adenoviridae*: the viruses and their replication, p. 2265–2300. *In* D. M. Knipe and P. M. Howley (ed.), Fields virology. Lippincott Williams & Wilkins, Philadelphia, Pa.
40. **Shpetner, H. S., B. M. Paschal, and R. B. Vallee.** 1988. Characterization of the microtubule-activated ATPase of brain cytoplasmic dynein (MAP 1C). J. Cell Biol. **107:**1001–1009.
41. **Sodeik, B.** 2000. Mechanisms of viral transport in the cytoplasm. Trends Microbiol. **8:**465–472.
42. **Spector, I., N. R. Shochet, Y. Kashman, and A. Groweiss.** 1983. Latrunculins: novel marine toxins that disrupt microfilament organization in cultured cells. Science **219:**493–495.
43. **Suomalainen, M., M. Y. Nakano, S. Keller, K. Boucke, R. P. Stidwill, and U. F. Greber.** 1999. Microtubule-dependent plus and minus end-directed motilities are competing processes for nuclear targeting of adenovirus. J. Cell Biol. **144:**657–672.
44. **Sussenbach, J. S.** 1967. Early events in the infection process of adenovirus type 5 in HeLa cells. Virology **33:**567–574.
45. **Thyberg, J., and S. Moskalewski.** 1999. Role of microtubules in the organization of the Golgi complex. Exp. Cell Res. **246:**263–279.
46. **Tomko, R. P., R. Xu, and L. Philipson.** 1997. HCAR and MCAR: the human and mouse cellular receptors for subgroup C adenoviruses and group B coxsackieviruses. Proc. Natl. Acad. Sci. USA **94:**3352–3356.
47. **Trotman, L. C., N. Mosberger, M. Fornerod, R. P. Stidwill, and U. F. Greber.** 2001. Import of adenovirus DNA involves the nuclear pore complex receptor CAN/Nup214 and histone H1. Nat. Cell Biol. **3:**1092–1100.
48. **Wang, K., S. Huang, A. Kapoor-Munshi, and G. Nemerow.** 1998. Adenovirus internalization and infection require dynamin. J. Virol. **72:**3455–3458.
49. **Wickham, T. J., P. Mathias, D. A. Cheresh, and G. R. Nemerow.** 1993. Integrins alpha v beta 3 and alpha v beta 5 promote adenovirus internalization but not virus attachment. Cell **73:**309–319.
50. **Wickham, T. J., E. J. Filardo, D. A. Cheresh, and G. R. Nemerow.** 1994. Integrin alpha v beta 5 selectively promotes adenovirus mediated cell membrane permeabilization. J. Cell Biol. **127:**257–264.
51. **Wisnivesky, J. P., P. L. Leopold, and R. G. Crystal.** 1999. Specific binding of the adenovirus capsid to the nuclear envelope. Hum. Gene Ther. **10:**2187–2195.